11th World Congress on Computational Mechanics (WCCM XI)
5th European Conference on Computational Mechanics (ECCM V)
6th European Conference on Computational Fluid Dynamics (ECFD VI)
E. Oñate, J. Oliver and A. Huerta (Eds)

# SIMULATION OF ARTERIAL WALLS UNDER CONSIDERATION OF RESIDUAL STRESSES - A NUMERICAL APPROACH

**JÖRG SCHRÖDER*, SARAH BRINKHUES* DOMINIK BRANDS* and MARKUS VON HOEGEN***

* Institute of Mechanics, Faculty of Engineering / Dept. Civil Engineering
University of Duisburg-Essen
Universitätsstr. 15, 45141 Essen, Germany
e-mail: j.schroeder@uni-due.de, web page: http://www.uni-due.de/mechanika/

**Key words:** Biomechanics, Residual Stresses, Stress Invariants, Patient-Specific Artery

**Abstract.** Experimental studies indicate that residual stresses are present in arterial walls. They reduce the circumferential stresses gradient in radial direction. In this contribution a method to smooth the stress gradient is presented in order to describe an accurate stress distribution. Suitable invariants are defined, averaged in sectors and transformed to a tensorial representation. The residual stresses are then subtracted from the loaded, non residually stressed, artery. The algorithmic treatment of this method is demonstrated for a 2D patient-specific hyperelastic model under plane strain conditions. The effect of different mesh densities is investigated.

## 1 INTRODUCTION

If an unloaded arterial wall is radially sliced, it will open up into a horseshoe. This experiment performed by Vaishnav and Vossoughi [20] and Chuong and Fung [5] is the proof for the existence of residual stresses in arteries. It can be shown that even the opened configuration is not stress free, which means when the body is sliced a second or third time the artery will slightly continue to deform, see Vossoughi et al. [21]. In the past many researches dealt with the question of the origin of these phenomenon and tried to derive models to determine the magnitude of the resulting stresses. It is well known that residual stresses significantly affect the 3D physiological stress distribution. Chuong and Fung [6] showed that the circumferential stress gradient is reduced throughout the vessel wall. Based on that Takamizawa and Hayashi [19] deduced a model including a uniform strain hypothesis for the circumferential strain.

A bundle of factors was discovered to give rise to residual stresses. It covers inter alia: growth and remodeling processes [4], muscle tone [23], osmotic swelling [10] or the blood pressure and hypertrophy [7]. In this research we restrict ourselves to accurately describe the stress distribution without explicitly simulating the mentioned reasons. In literature we already find several numerical approaches to incorporate residual stresses. Wang et al. [22] modify the free energy so that it directly contains the residual strains. Rausch and Kuhl [13] use an multiplicative split of the deformation gradient into residually and load induced gradients based on a in-plane prestretch. Likewise the publication of Ståhlhand et al. [18] deals with prestrain deformation gradients depending on the opening angle. Growth models can be found in Menzel [11] or Polzer et al. [12], for instance.

## 2 MATERIAL MODELLING OF SOFT BIOLOGICAL TISSUES

The material behavior of arterial walls is transversely isotropic in general. Bundles of collagen fibers are crosswise orientated in preferred directions. Therefore we consider the structural tensor

$$\boldsymbol{M}_{(a)} = \boldsymbol{A}_{(a)} \otimes \boldsymbol{A}_{(a)} \qquad \text{with} \qquad \operatorname{tr} \boldsymbol{M}_{(a)} = 1 \quad \text{and} \quad \|\boldsymbol{A}_{(a)}\| = 1, \tag{1}$$

where $\boldsymbol{A}_{(a)}$ is a direction vector in the reference configuration taking two fiber orientations $a = 1, 2$ into account. The used free energy function depend on both, the Cauchy-Green tensor $\boldsymbol{C} = \boldsymbol{F}^T \boldsymbol{F}$, where $\boldsymbol{F}$ is the deformation gradient, and on $\boldsymbol{M}$. The deformation gradient itself is defined as $\boldsymbol{F} = \operatorname{Grad} \boldsymbol{\varphi}(\boldsymbol{X})$, where $\boldsymbol{X}$ represents the reference configuration and $\boldsymbol{\varphi}(\boldsymbol{X})$ the motion with respect to the reference configuration. Throughout this work we use polyconvex energy functions, which satisfy the Legendre-Hadamard condition and therefore ensure real wave speeds, in the form

$$\psi = \psi(I_1, I_2, I_3, J_4^{(a)}, J_5^{(a)}), \tag{2}$$

where $I_1 = \operatorname{tr} \boldsymbol{C}$, $I_2 = \operatorname{tr}[\operatorname{cof} \boldsymbol{C}]$ and $I_3 = \det \boldsymbol{C}$ are the invariants of $\boldsymbol{C}$. The mixed invariants of $\boldsymbol{C}$ and $\boldsymbol{M}$ are

$$J_4^{(a)} = \operatorname{tr}[\boldsymbol{C}\boldsymbol{M}_{(a)}] \qquad \text{and} \qquad J_5^{(a)} = \operatorname{tr}[\boldsymbol{C}^2\boldsymbol{M}_{(a)}], \tag{3}$$

see Boehler [2]. Furthermore the free energy is split into an isotropic part $\psi^{iso}$ representing the matrix material and a transversely isotropic part $\psi^{ti}$ for the fibers. The existence of mainly two present fiber directions $\boldsymbol{A}_{(a)}$ yields

$$\psi(I_1, I_2, I_3, J_4^{(a)}, J_5^{(a)}) = \psi^{iso}(I_1, I_2, I_3) + \sum_{a=1}^{2} \psi^{ti}(I_1, I_2, I_3, J_4^{(a)}, J_5^{(a)}), \tag{4}$$

which is a superposition of two transversely isotropic models, cf. Holzapfel et al. [8]. For the isotropic part the coercive, polyconvex and compressible Mooney-Rivlin model is chosen:

$$\psi^{iso} = c_1 I_1 + c_2 I_2 + c_3 I_3 - \delta \ln \sqrt{I_3}. \tag{5}$$

A function for the transversely isotropic part of the free energy in Eq. (4) which is suitable to describe the strong stiffening effect caused by high loading in biological tissues is given in Holzapfel et al. [8]:

$$\psi^{ti}_{(a)} = \frac{k_1}{2k_2} \left\{ \exp\left[ k_2 \langle J_4^{(a)} - 1 \rangle^2 \right] - 1 \right\} \quad \text{for} \quad a = 1, 2 \, . \tag{6}$$

The invariant $J_4^{(a)}$ can be interpreted as the square of the stretch in the corresponding fiber direction. Eq. (6) includes the assumption that fiber stresses only result from elongations in the corresponding direction. Because of that the anisotropic term can be neglected in case of fiber compression due to buckling of the fibers. As a consequence, for $J_4^{(a)} \leq 1$, the term inside the Macaulay brackets becomes zero and therefore the whole energy function is reduced to the isotropic part. The choice of the material parameters $k_1$ and $k_2$ have to be adjusted to the assumption that the fibers are the main stiffness providing components of the arterial wall. While $k_2$ is dimensionless $k_1$ is a stress like parameter.

In the following sections the artery will be subdivided into three material components, i.e. media, adventitia and plaque. The plaque composition differs depending on the patient and few experimental data is available so that we assume a homogenous and isotropic body. Therefore we only make use of the Mooney-Rivlin model, see Eq. (5). The parameters were gained on the basis of the Lamé constants $\mu$ and $\lambda$. The parameters were selected in such a way that the plaque is also quasi incompressible, a Poisson's ratio $\nu$ of 0.478 is postulated, and are shown in Table 1. In contrast, however, media and adventitia behave anisotropic and the full free energy function in Eq. (4) is used for both of them. The described model was adjusted to experimental data obtained from uniaxial tension tests, see Holzapfel et al. [9]. To account for the anisotropic behavior therein sample stripes were cut out in radial and circumferential direction and the layers were tested separately. As explained in Schroeder and Brinkhues [16] the parameter identification gives two different parameter sets, one for media and one for adventitia, which are shown in Table 2. Here $2\beta_f$ represents the angle between the fiber directions of the specific layer. A least square method was used to minimize the error between experiments and simulation, for a details see [3] and [1].

Table 1: Material parameters for the plaque.

| $\lambda$/kPa | $\mu$/kPa | $c_1$/kPa | $c_2$/kPa | $c_3$/kPa | $\kappa_{al}$ |
|---|---|---|---|---|---|
| 3259.0 | 150.0 | 60.0 | 15.0 | 800.0 | 999.0 |

Table 2: Material parameters for the media and the adventitia.

| | $c_1$/kPa | $c_2$/kPa | $c_3$/kPa | $k_1$/kPa | $k_2$/- | $\beta_f/^\circ$ | $\kappa_{al}$ |
|---|---|---|---|---|---|---|---|
| media | 14.638 | 0.149 | 60.810 | 6.851 | 754.014 | 43.468 | 99.0 |
| adventitia | 2.326 | 6.169 | 60.642 | $3.131 \cdot 10^{-8}$ | 147.174 | 52.285 | 99.0 |

# 3 INCORPORATION OF RESIDUAL STRESSES

In [16] and [3] a method is proposed based on the assumption that residual stresses reduce the gradient of the wall stress in radial direction. The idea is to use the local difference of the fiber stresses with respect to its volume average for the estimation of the residual stresses. Since arterial walls exhibit a distinct material behavior in fiber direction, the fiber stress was chosen as a scalar stress measure. The numerical realization of this method is done on a decomposition of the domain into segments, as schematically shown in Fig. 1.

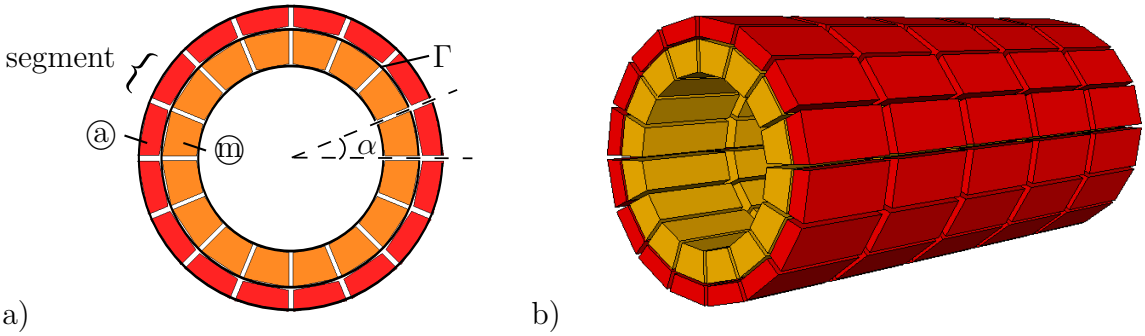


a) b)

Figure 1: Schematic illustration of the decomposition of an arterial cross-section, which consists of two materials (media ⓜ and adventitia ⓐ, i.e. $\mathrm{n_{MAT}} = 2$), here $\mathrm{n_{SG}} = 16$; two-dimensional cross-section decomposed into $\mathrm{n_{SC}^{2D}} = 32$ sectors and b) additional longitudinal decomposition in $\mathrm{n_L} = 5$ parts yielding $\mathrm{n_{SC}^{3D}} = 32 \cdot 5 = 160$ sectors.

Under consideration of a cross-section consisting of $\mathrm{n_{MAT}}$ layers or materials, respectively, which is divided into $\mathrm{n_{SG}}$ segments, the number of sectors can be specified as

$$\mathrm{n_{SC}^{2D}} = \mathrm{n_{SG}} \cdot \mathrm{n_{MAT}} \quad \text{and} \quad \mathrm{n_{SC}^{3D}} = \mathrm{n_{SG}} \cdot \mathrm{n_{MAT}} \cdot \mathrm{n_L} \ , \tag{7}$$

for two- and three-dimensional geometries respectively. The consideration of three-dimensional numerical simulations requires an additional decomposition in $\mathrm{n_L}$ longitudinal segments. It is reasonable to subdivide the segments into sectors with respect to the material interfaces since the layers provide different stiffnesses and the opening angle of the separated layers is different. As a consequence the residual stress distribution is also different. Due to the rotatory structure of the artery it is clear that the radial stresses at the interface $\Gamma$ will be equal. This is not the case for the circumferential stresses in radial direction, where we obtain a discontinuity at the interface. Decomposition is applied with

respect to the elements which means that each Gauss-point of an element belongs to the same segment.

The Cauchy-stresses of quasi-incompressible materials that exhibit distinct behavior in preferred directions can be additively decomposed into deviatoric ground stresses $\boldsymbol{\sigma}^*$ and reaction stresses $\boldsymbol{\sigma}^r$, i.e.

$$\boldsymbol{\sigma} = \boldsymbol{\sigma}^* + \boldsymbol{\sigma}^r \ . \tag{8}$$

Since the material is assumed to be incompressible and inextensible in the current fiber directions $\boldsymbol{a}_1$ and $\boldsymbol{a}_2$ the reaction to the constraints

$$\boldsymbol{\sigma}^r = -p\ \mathbf{1} + T_{(1)}\ \tilde{\boldsymbol{m}}_{(1)} + T_{(2)}\ \tilde{\boldsymbol{m}}_{(2)} \tag{9}$$

includes the hydrostatic pressure $p$ and the fiber-stresses $T_{(1)}$ and $T_{(2)}$. Here, $\tilde{\boldsymbol{m}}_{(1)}$ and $\tilde{\boldsymbol{m}}_{(2)}$ are the structural tensors for the normalized actual preferred directions $\tilde{\boldsymbol{a}}_{(a)}$ given by

$$\tilde{\boldsymbol{m}}_{(a)} = \tilde{\boldsymbol{a}}_{(a)} \otimes \tilde{\boldsymbol{a}}_{(a)} \quad \text{with} \quad \tilde{\boldsymbol{a}}_{(a)} = \frac{\boldsymbol{a}_{(a)}}{||\boldsymbol{a}_{(a)}||} \quad \text{and} \quad \boldsymbol{a}_{(a)} = \boldsymbol{F}\boldsymbol{A}_{(a)} \quad \text{for} \quad a = 1, 2\ . \tag{10}$$

Using the side conditions $\mathrm{tr}\boldsymbol{\sigma}^* = 0$, $\boldsymbol{\sigma}^* : \tilde{\boldsymbol{m}}_{(1)} = 0$ and $\boldsymbol{\sigma}^* : \tilde{\boldsymbol{m}}_{(2)} = 0$, the fiber stresses and the hydrostatic pressure in an arbitrary stress state can be expressed through

$$\begin{aligned}
p \quad &= \big[\, -(\xi+1)\ \mathbf{1} : \boldsymbol{\sigma} \ + \qquad\qquad \boldsymbol{\sigma} : \tilde{\boldsymbol{m}}_{(1)} \ + \qquad\qquad \boldsymbol{\sigma} : \tilde{\boldsymbol{m}}_{(2)} \ \big] \,/\, \big[3\xi + 1\big]\ , \\
T_{(1)} &= \big[ \quad (1-\xi)\ \mathbf{1} : \boldsymbol{\sigma} \ - \qquad 2\ \boldsymbol{\sigma} : \tilde{\boldsymbol{m}}_{(1)} \ + \ (3\,\xi - 1)\ \boldsymbol{\sigma} : \tilde{\boldsymbol{m}}_{(2)} \ \big] \,/\, \Xi\ , \\
T_{(2)} &= \big[ \quad (1-\xi)\ \mathbf{1} : \boldsymbol{\sigma} \ + \ (3\,\xi - 1)\ \boldsymbol{\sigma} : \tilde{\boldsymbol{m}}_{(1)} \ - \qquad 2\ \boldsymbol{\sigma} : \tilde{\boldsymbol{m}}_{(2)} \ \big] \,/\, \Xi\ .
\end{aligned} \tag{11}$$

Here, the abbreviations $\xi = \tilde{\boldsymbol{m}}_{(1)} : \tilde{\boldsymbol{m}}_{(2)} = \cos^2\phi$ and $\Xi = 3\,\xi^2 - 2\,\xi - 1$ are introduced, where $\phi$ denotes the inclination angle between the two current preferred directions. The general idea of this approach is based on Spencer [17] and Roger [14], see also Schröder [15]. Based on the aforementioned relations and assumptions a calculation procedure to account for residual stresses is presented:

- radial segmentation of the geometry in material sections
- apply internal blood pressure and calculate $\boldsymbol{\sigma}$ and $\boldsymbol{S}$ respectively
- apply smoothing loops (SL):
  a) calculate mean fiber stresses $\overline{T}^{\,i}_{(a)}$ in each sector domain $\mathcal{B}_i$ with respect to the volume

$$\overline{T}^{\,i}_{(a)} = \frac{1}{V_i} \int\limits_{\mathcal{B}_i} T_{(a)}(\boldsymbol{x})\ \mathrm{d}v \quad \text{in } \mathcal{B}_i \tag{12}$$

b) subtract the sector mean values from the fiber stresses and calculate the deviation of the hydrostatic pressure on each Gauss-point belonging to the specific sector

$$\Delta T_{(a)} = T_{(a)} - \overline{T}^{i}_{(a)} \quad \text{in } \mathcal{B}_i; \quad \Delta p = \frac{1}{3}\left(\Delta T_{(1)} + \Delta T_{(2)}\right) \tag{13}$$

c) transform the deviation of the fiber stresses to a tensorial representation, i.e. the residual stresses, with help of Eq. (9)

$$\boldsymbol{\sigma}^{\text{res}} = -\Delta p\, \mathbf{1} + \sum_{a=1}^{2} \Delta T_{(a)}\, \tilde{\boldsymbol{m}}_{(a)} \tag{14}$$

d) map residual stresses to the reference configuration, subtract them from the previous stress state and iterate a new equilibrium for the physiological stress state $\boldsymbol{S}^{\text{phys}}$

$$\boldsymbol{S}^{\text{res}} := J\boldsymbol{F}^{-1}\,\boldsymbol{\sigma}^{\text{res}}\,\boldsymbol{F}^{-T}; \quad \boldsymbol{S}^{\text{phys}} = \boldsymbol{S} - \tilde{\lambda}\boldsymbol{S}^{\text{res}} \tag{15}$$

The smoothing loops (SL) are repeated several times. A stopping criterion has to be defined. In order to derive $\Delta p$ it was assumed that $\text{tr}\boldsymbol{\sigma}^{\text{res}} = 0$ . For the very last step of the smoothing loop the proportionate factor $\tilde{\lambda} \in [0, 1]$ is introduced in order to subtract only a fraction of the residual stresses.

## 4 2D PATIENT-SPECIFIC ARTERY EXAMPLE

As a numerical example the geometry depicted in Fig. 2a was meshed with 6015, 12119 and 23245 six-noded triangular elements with quadratic shape functions respectively. Fig. 2b shows the decomposition of the geometry into 36 segments and 72 sectors and the applied boundary conditions. Note that no sectors have been assigned for the plaque, i.e no smoothing is applied on this layer. In addition the sections A-A and B-B for the later shown results are introduced.

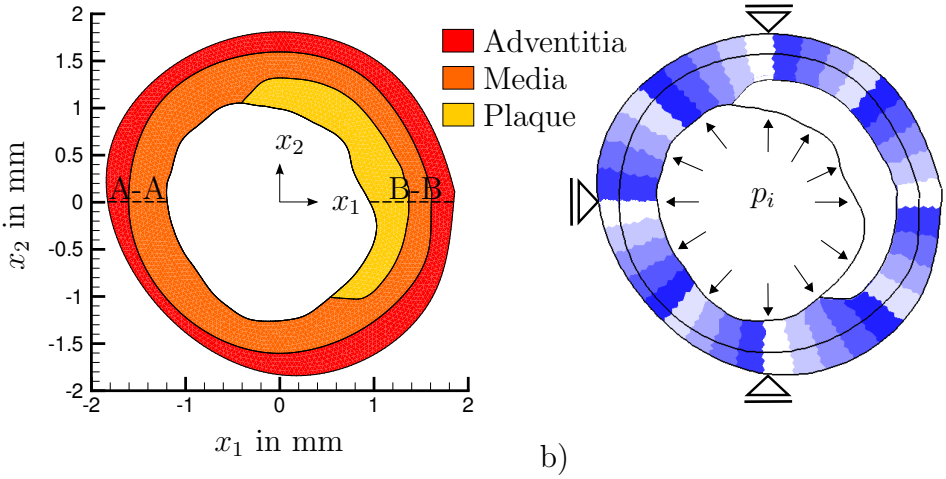


Figure 2: a) Geometry of a patient-specific arterial wall composed of adventitia, media and plaque and b) decomposition into $n^{2D}_{SC} = 36 \cdot 2$ sectors and applied boundary conditions.

According to the calculation scheme described in Section 3 the vessel is first loaded with an internal pressure $p_\mathrm{i}$ of 16 kPa. After that 10 smoothing loops (SL) with an proportionate factor of $\tilde{\lambda} = 0.1$ were applied. The results for $T_{(1)}$ in section A-A for the three different meshes are plotted in Fig. 3. For the plot all Gauss-points were evaluated within a tolerance angle of 0.7° for the upper sector bordering A-A. For each mesh the effect of the smoothing loop is obvious and the stress distribution becomes more uniform. Due to the fact that the stresses in the adventitial layer are close to zero and already nearly equally distributed the smoothing effect is comparatively small. Moreover it is visible from the results obtained using the coarse mesh that especially the smoothing procedure requires a higher mesh density. The maximum value in $T_{(1)}$ differs by more than 20 kPa after smoothing, while the curves of the two denser meshes do not deviate much from each other.

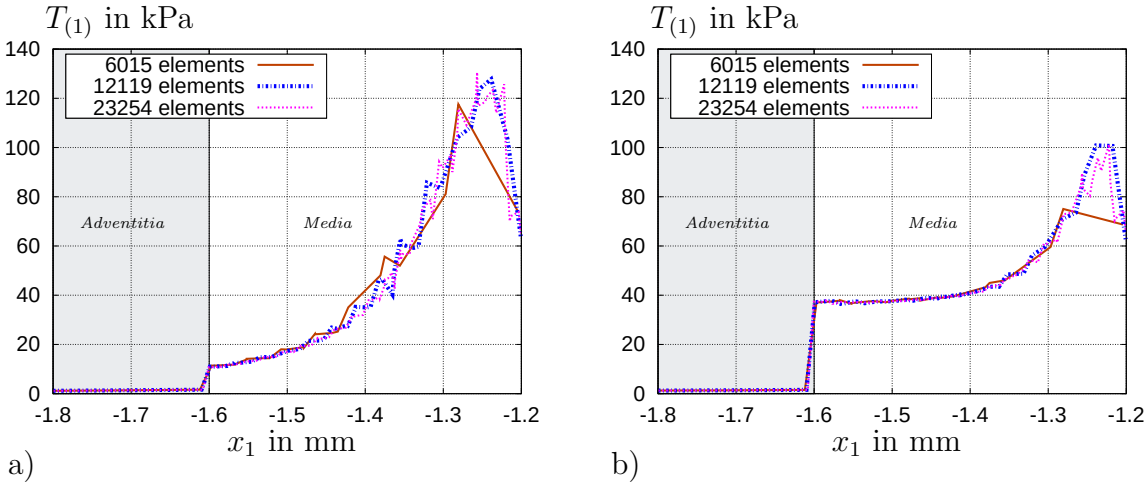


Figure 3: Distribution of the fiber stress $T_{(1)}$ across the wall thickness in section A-A on the left hand side, a) without residual stresses and b) after application of 10 SL.

In Fig. 4 the Cauchy-stresses $\sigma_{11}$, $\sigma_{22}$ and $\sigma_{33}$ of the calculation using 23254 elements are depicted for section A-A and B-B, respectively. For these special sections the depicted stresses coincide with the radial, circumferential and longitudinal stress components, respectively. The smoothing effect is clearly visible for the circumferential stresses $\sigma_{22}$ and the longitudinal stresses $\sigma_{33}$, i.e. the stress gradient decreases. Because of the difference in stiffness of the layers the line graphs display sudden rises in stress at the point of the interface. That was the reason why the sectors for the averaging method were not only defined by the angle but also by the material interfaces. As the fibers are only orientated in circumferential and longitudinal direction the changes of the radial stresses are rather small. Because of the equilibrium constraints of rotational solids for the radial stresses no jumps occur at the layer interfaces and on the outermost layer they have to be zero. In section B-B three material layers are present. As no smoothing is applied to the plaque, only slight changes occur in this layer.

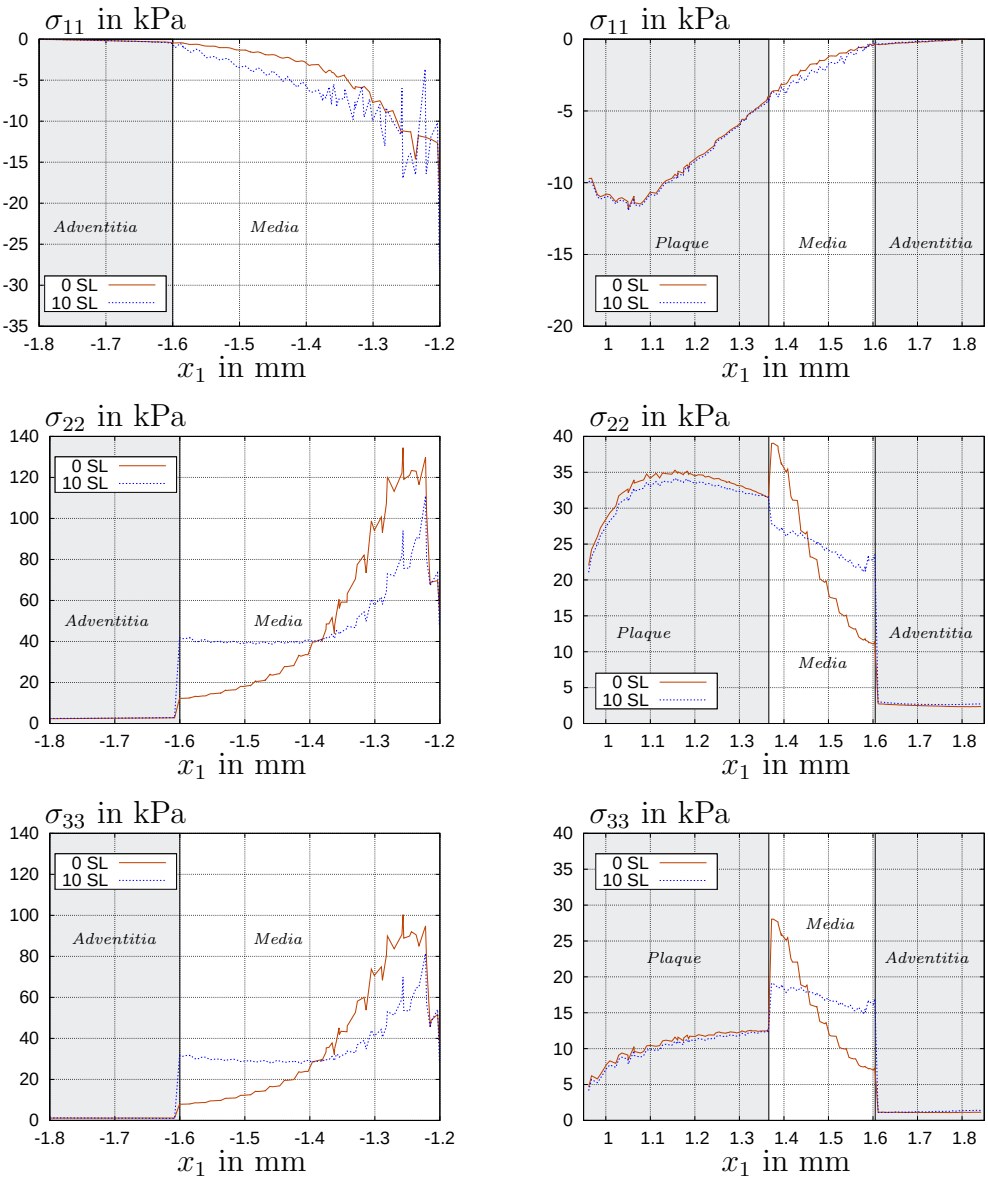


Figure 4: Gauss-point plot of the Cauchy-stresses $\sigma_{11}$, $\sigma_{22}$ and $\sigma_{33}$ across the wall thickness in section A-A on the left hand side and B-B on the right hand side corresponding to their definition in Fig. 2 and using the fine mesh (23254 elements).

The calculated residual stresses, as shown above, were then applied on the unloaded body. A cut was applied at the bottom of the artery at a position of $x_1 = 0$ in the reference configuration. In Fig. 5 the deformations of the coarse and the fine mesh are compared. As it can be seen the artery opens as it is reported in literature. Concerning the mesh density the difference is small in this case. It seems, that the stress differences,

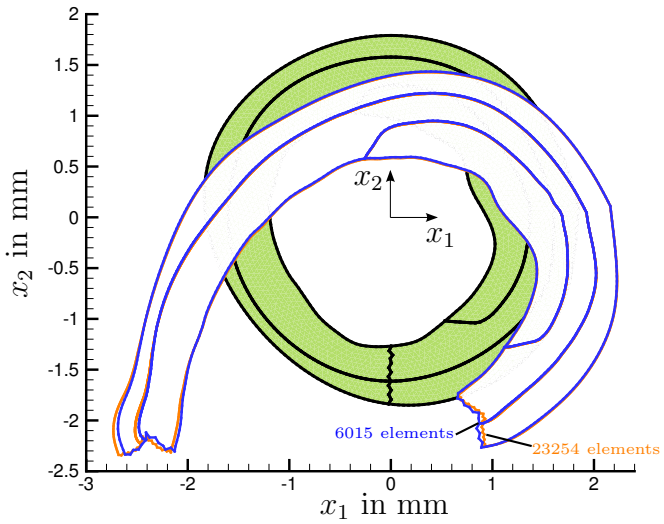


Figure 5: Comparison of the deformed configurations of the open-angle experiment simulation for the coarse mesh (6015 elements) and the fine mesh (23254 elements).

regarding the mesh density in the inner region of the medial layer, shown in Fig 3b, have only a lower influence on the open-angle experiment. Moreover the influence of the plaque is visible. Because of the stiffness providing plaque the opening to the left is more pronounced than to the right side.

In Fig. 6 the von-Mises stress distribution in different situations of the presented approach are shown. The stress concentration near the inner region of the medial layer for the loaded non-residually stressed artery, cf. Fig. 6a, is obviously reduced after the smoothing operation, cf. Fig. 6b. As shown in Fig. 6c the opened artery is not stress free,

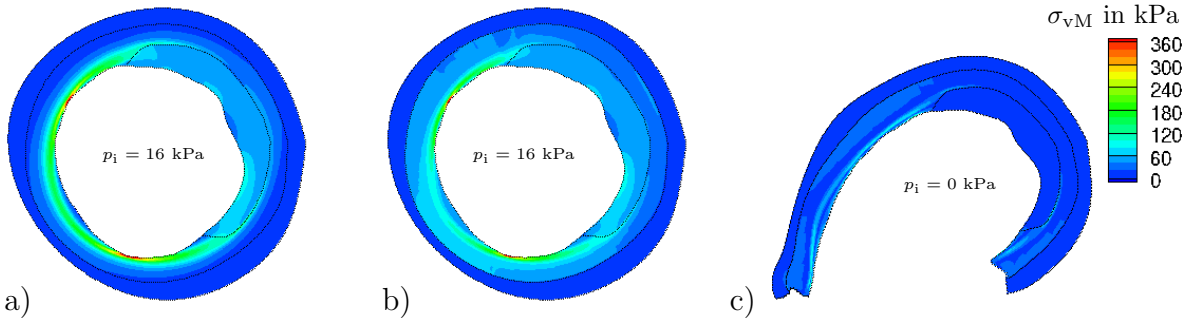


Figure 6: Contour plot of the von Mises stresses $\sigma_{\mathrm{vM}}$ for a) the loaded, non-residually stressed artery, b) the loaded artery after 10 SL and c) the non-loaded artery after opening for the fine mesh (23254 elements).

# 5 CONCLUSION

Residual stresses can be approximated by smoothing the circumferential stress gradient. The fiber stresses are suitable scalar stress measures in this context. A method to smooth and project them onto the current preferred direction was derived and discussed for a patient-specific artery. The next steps should be the extension of the presented scheme to three-dimensional problems and the comparison with a strain based approach.

# REFERENCES

[1] Balzani, D. and Brinkhues, S. and Holzapfel, G.A. Constitutive framework for the modeling of damage in soft biological tissues. *Comput. Methods Appl. Mech. Engrg.* (2012) **213–216**:139–151.

[2] Boehler, J.P. Introduction to the invariant formulation of anisotropic constitutive equations. In Boehler, J.P., editor, *Applications of Tensor Functions in Solid Mechanics*(1987) number 292.

[3] Brinkhues, S. Modeling and simulation of arterial walls with focus on damage and residual stresses. PhD thesis, *Institute of Mechanics, Department of Civil Engineering, Faculty of Engineering, University of Duisburg-Essen* (2012).

[4] Cardamone, L. Valentin, A. Eberth, J.F. and Humphrey, J.D. Origin of axial prestretch and residual stress in arteries. *Biomech. Model. Mechanobiol.* (2009), **8**:431–446.

[5] Choung ,C.J. and Fung, Y.C. Three-dimensional stress distribution in arteries. *J. Biomech. Eng.* (1983) **108**:189-192

[6] Chuong, C.J. and Fung, Y.C. On residual stress in arteries. *J. Biomech. Eng.* (1986) **108**:189–191.

[7] Fung, Y.C. and Liu, S.Q. Change of residual strains in arteries due to hypertrophy caused by aortic constriction. *Circ. Res.* (1989) **65**:1340–1349.

[8] Holzapfel, G.A. and Gasser, T.C. and Ogden, R.W. A new constitutive framework for arterial wall mechanics and a comparative study of material models. *J. Elast.* (2000) **61**:1–48.

[9] Holzapfel, G.A. Sommer, G. and Regitnig, P. Anisotropic mechanical properties of tissue components in human atherosclerotic plaques. *J. Biomech. Eng.* (2004) **126**:657–665.

[10] Lanir, Y. Osmotic swelling and residual stress in cardiovascular tissues. *J. Biomech.* (2012) **45**:780–789.

[11] Menzel, A. A fibre reorientation model for orthotropic multiplicative growth. *Biomech. Model. Mechanobiol.* (2007) **6**:303–320.

[12] Polzer, S. Bursa, J. Gasser, T.C. Staffa, R. and Vlachovsky, R. A numerical implementation to predict residual strains from the homogeneous stress hypothesis with application to abdominal aortic aneurysms. *Ann. Biomed. Eng.* (2013) **41**:1516-1527.

[13] Rausch, M.K. and Kuhl, E. On the effect of prestrain and residual stress in thin biological membranes. *J. Mech. Phys. Solids* (2013) **61**:1955–1969.

[14] Rogers, T.G. Yield criteria, flow rules, and hardening in anisotropic plasticity In Boehler, J.P., editor, *Yielding, damage and failure of anisotropic solids* (1987).

[15] Schröeder, J. Theoretische und algorithmische Konzepte zur phänomenologischen Beschreibung anisotropen Materialverhaltens. PhD thesis, *Universität Hannover, Institut für Mechanik (Bauwesen), Lehrstuhl I* (1996).

[16] Schröder, J. and Brinkhues, S. A novel numerical scheme for the computation of residual stresses in arterial walls. *Biomech. Model. Mechanobiol.* (2014) in press.

[17] Spencer, A.J.M. *Deformations of fibre-reinforced materials*. Oxford University Press, Vol. I., (1972).

[18] Ståhlhand, J. Klarbring, A. and Karlsson, M. Towards in vivo aorta material identification and stress estimation. *Biomech. Model. Mechanobiol.* (2004) **2**:169–186.

[19] Takamizawa, K. and Hayashi, K. Strain energy density function and uniform strain hypothesis for arterial mechanics. *J. Biomech.* (1987) **20**:7–17.

[20] Vaishnav, R.N. and Vossoughi, J. Estimation of residual strains in aortic segments. In C.W. Hall, editor, *Biomedical Engineering II: Recent Developments*. Pergamon Press, New York, (1983).

[21] Vossoughi, J. Hedjazi, Z. and Borris. F.S. Intimal residual stress and strain in large arteries. In N.A. Langrana, M.H. Friedman, and E.S. Grood, editors, *Proceedings of the Summer Bioengineering Conference, New York*, American Society of Mechanical Engineers (1993): 434–437.

[22] Wang, H.M. Luo, X.Y. Gao, H. Ogden, R.W. Griffith, B.E. Berry, C. T. and Wang, J. A modified Holzapfel-Ogden law for a residually stressed finite strain model of the human left ventricle in diastole. *Biomech. Model. Mechanobiol.* (2014) **13**:99-113.

[23] P.J. Zeller, P.J. and Skalak, T.C. Contribution of individual structural components in determining the zero-stress state in small arteries. *J. of Vasc. Res.* (1998) **35**:8–17.